Article

A Numerical Analysis of Dynamic Slosh Dampening Utilising Perforated Partitions in Partially-Filled Rectangular Tanks

Mitchell G. Borg [1,*], Claire DeMarco Muscat-Fenech [1,*], Tahsin Tezdogan [2], Tonio Sant [1], Simon Mizzi [1] and Yigit Kemal Demirel [2]

[1] Department of Mechanical Engineering, University of Malta, MSD2080 Msida, Malta; tonio.sant@um.edu.mt (T.S.); simon.mizzi@um.edu.mt (S.M.)

[2] Department of Naval Architecture, Ocean, and Marine Engineering, University of Strathclyde, Glasgow G4 0LZ, UK; tahsin.tezdogan@strath.ac.uk (T.T.); yigit.demirel@strath.ac.uk (Y.K.D.)

* Correspondence: mitchell.borg@um.edu.mt (M.G.B.); claire.demarco@um.edu.mt (C.D.M.-F.)

Abstract: Conventional liquefied natural gas (LNG) cargo vessels are imposed with tank-fill limitations as precautions to prevent structural damage and stability-loss due to high-impact sloshing, enforcing cargo volume-fills to be lower than 10% or higher than 70% of the tank height. The restrictions, however, limit commercial operations, specifically when handling spot trades and offshore loading/unloading at multiple ports along a shipping route. The study puts forward a computational fluid dynamic (CFD) sloshing analysis of partially-filled chamfered rectangular tanks undergoing sinusoidal oscillatory kinetics with the use of the explicit volume-of-fluid and non-iterative time-advancement schemes utilising the commercial solver ANSYS-Fluent. Establishing a 20% to 60% fill-range, the sloshing dynamics were acknowledged within an open-bore, partitioned, and perforated-partitioned tank when oscillating at frequencies of 0.5 Hz and 1 Hz. The overall torque and static pressure induced on the tank walls were investigated. High-impact slamming at the tank roof occurred at 40% and 60% fills, however, the implementation of the partition and perforated-partition barriers successfully reduced the impact due to suppression and dissipation of the wave dynamics.

Keywords: sloshing; pendulum oscillation; rectangular tank; CFD; NITA; VOF

1. Introduction

Extreme ship motions encountered during rough sea conditions while transporting liquid cargo within partially-filled tanks may induce substantial dynamic loads, which may be detrimental to vessel seakeeping and manoeuvrability. Attributable to the partially-filled multiphase domain, external forces acting upon the vessel tank shift the liquid-phase from an equilibrium state, displacing the centre of mass and free-surface, characterising the sloshing phenomenon [1]. Significant sloshing dynamics within liquefied natural gas (LNG) cargo tanks may result in breaking waves that potentially bring about structural damage and stability loss due to high-impact slamming [2,3]. Consequently, the introduction of tank-fill limitations has, for many years, been acknowledged as an essential precautionary measure to prevent engineering repercussions due to sloshing. The imposed limitations constrain the cargo volume-fill to be either lower than 10% or higher than 70% of the tank height [2]. The restrictions, however, limit commercial operations, distinctively when handling spot trades and offshore loading/unloading at multiple ports along a shipping route.

In utilising linear theoretical sloshing analysis, Budiansky [4] established that the fundamental frequency of the sloshing dynamics increased in a monotonic manner with increasing fill-volumes for fill-levels of less than 60%, but attained an increased rate-of-change at higher fills. Abramson [5] correspondingly concluded that the tank fill-volume

is a contributing factor in establishing the natural frequency of the liquid-slosh motion for various tank configurations. Considering sloshing investigations by means of a pendulum-equivalent mechanical system model, Slibar and Troger [6] studied liquid sloshing utilising a single degree-of-freedom mechanical oscillator to compute the fluid dynamics. Furthermore, Ranganathan [7] modelled large-amplitude non-linear liquid-sloshing within horizontal partially-filled cylindrical cargo-tanks coupled with dynamic roll accelerations, whereas Salem et al. [8] indicated that the magnitude of the accelerations induced was a characteristic factor in the liquid-response. Gabl et al. [9] also investigated a cylindrical tank, which was free floating to provide an experimental investigation of a fluid–structure–fluid interaction.

In establishing a computational fluid dynamic (CFD) methodology for seafaring sloshing investigations, Celebi and Akyildiz [10] investigated non-linear liquid sloshing inside a partially-filled rectangular tank. Tank kinetics were induced harmonically to simulate a rolling motion. The model solved the Navier–Stokes equations by implementing finite-difference approximations whilst utilising the volume-of-fluid (VOF) technique to track the free surface. In continuation, Akyildiz [11] investigated the roll dynamics of a partially-filled rectangular tank with a vertical baffle by varying the ratio of baffle height to initial liquid depth. He et al. [12] conducted a validation experiment for rectangular tanks and beam waves. Bulian et al. [13] developed a six degree-of-freedom (DOF) ship motion numerical solver by coupling rigid-body dynamics and external fluid-structure interaction with a smoothed-particle hydrodynamics solver to analyse the internal sloshing dynamics. Thiagarajan et al. [14] carried out numerical investigations on sloshing motions in a two-dimensional tank with fill-levels varying from 10% to 95% of the tank height, an oscillation frequency range of 0.35 Hz to 1.25 Hz, and a peak-to-peak displacement of 0.25 m. Utilising the finite-volume method coupled with the VOF technique, the computational results for free-surface elevation and impact pressure were found to be in good agreement with the experimentation. Good agreements could also be found for meshless numerical solutions based on smoothed particle hydrodynamics (SPH) [15–17].

In comparing planar baffle orientation, Liu and Lin [18] identified a vertical baffle to be more effective than a horizontal baffle in reducing the sloshing amplitude and decreasing the pressure exerted on the wall due to slamming. Jung et al. [19] investigated the variation in vertical baffle height on liquid sloshing in a laterally-moving rectangular tank. A correlation of baffle height to initial liquid height was acknowledged in establishing the critical baffle height at which tank roof impact was nulled. Yu et al. [20] investigated sloshing in a membrane-type LNG tank with two floating dampening plates under harmonic roll excitation. Lu et al. [21] developed a viscous fluid model for liquid sloshing in non-baffled and baffled rectangular tanks. The numerical study indicated the influence of the baffle width and position upon the sloshing response due to dissipative effects, where the sloshing in a baffled tank encompassed more dissipation due to stronger vortical flow in the vicinity of the baffle.

In modelling sloshing dynamics through perforated structures, Molin [22] proposed a theoretical model for slotted partitions based on non-linear sloshing mechanics. Faltisen et al. [23] modelled two-dimensional sloshing suppression in a partially-filled rectangular tank with a high-solidity slat-type screen undergoing simple harmonic motion. Molin and Remy [24] proposed the use of perforated vertical baffles as liquid dampers at the mid-length of partially-filled rectangular tanks to mitigate the vibratory sloshing response. Jin et al. [25] analysed the slosh dynamics within a partially-filled rectangular tank incorporated with a horizontal perforated plate to increase energy dissipation and diminish the pressure acting on the tank walls. The results established that horizontal perforated plates significantly restrain violent resonant sloshing in a tank under linear excitation.

The implementation of perforated partitions within a rectangular containment unit for the purpose of sloshing suppression has been established to be of particular interest due to its practical large-scale use and cost-effective simplicity in fabrication and installa-

tion. However, albeit the research undertaken, the efficacy of installing perforated partitions as tank architecture for slosh suppression by utilising high-fidelity numerical modelling has not been undertaken. Moreover, the literature has elaborated slosh dampening in terms of free-surface reduction and localised wall-pressure diminishment, however, utilising a pendulum model to determine the holistic torque variation induced by the fluid within the tank, rather than solely through qualitative or localised-quantitative data analysis, has not been tackled.

The paper elaborates a three-dimensional VOF-CFD approach, utilising the non-iterative time-advancement (NITA) technique, in modelling the dynamic sloshing torque within a rectangular containment unit with a perforated-partition when undergoing simple harmonic oscillatory motion. The study formed part of the 'DeSloSH' research project, which developed an experimentation and numerical framework for the suppression of sloshing within naval tankers by means of perforated-partitioned containment units when succumbing to oscillatory motion. In addition to the validation of an experimentation sloshing rig, the small-scale numerical analysis established the damping capacity upon the perforated-partition implementation for future numerical studies tackling true-scale vessel tank designs.

2. Numerical Methodology

2.1. Physical Setups

To validate a VOF-CFD numerical model for sloshing applications, simulations were carried out to numerically replicate theoretical values of an instantaneous turbulent dam break in a dry rectangular horizontal channel put forward by Chanson [26]. The fluid physics were established to be similar due to the dynamic, transient free-surface flow within a confined volume. The general dimensions of the channel included a length (L_c), height (H_c), and breadth (B_c) of 30 m, 0.30 m, and 0.60 m, respectively, as illustrated in Figure 1. Within the channel, the initially-static water reservoir dimensions included a length (L_r), height (H_r), and breadth ($B_r = 4H_r$) of 15 m, 0.15 m, and 0.60 m, respectively, attaining a Reynolds number of 1.81×10^5. The channel dimensions were implemented to acquire a wide semi-infinite reservoir with an analogous breadth-to-height cross-sectional length-scale to the sloshing tanks designed. The transient model was solved once the wave reached the channel end, approximately equivalent to 13 s, to attain an analogous time-scale to the oscillating tank model.
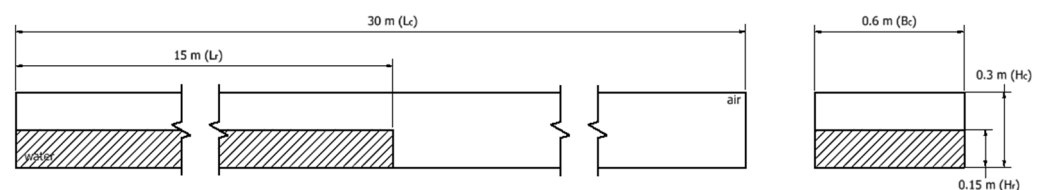
Figure 1. First-angle projection of the dam-break channel geometrical model; shaded volume represents the secondary-phase sub-domain.

In continuation, the tank geometrical models described three distinct setups to investigate distinct partition porosities: an open-bore tank (100% porosity), a partitioned tank (0% porosity), and a perforated-partitioned tank (50% porosity). The dimensions of the tanks described a length (L_t), height (H_t), and breadth (B_t) of 0.48 m, 0.23 m, and 0.20 m, respectively, as illustrated in Figure 2. Truncations at the tank length-to-height cross-section corners were imposed 0.05 m from the vertex at a 45° angle. The dimensions replicated physical experimentation conducted with a 2:1 length-to-height cross-sectional aspect ratio tank of 0.50 m by 0.25 m by 0.22 m, with a 10 mm tank-wall thickness. The partitioned tank model imposed a partition plate of 10 mm thickness along the vertical symmetrical plane, as displayed in Figure 3. The perforated-partitioned model utilised an identical partition plate, but incorporated 295 orifices with a 10 mm diameter to impose a

50% porosity partition, as illustrated in Figure 4. The orifice configuration followed a triangular layout, with a lateral displacement of 12 mm between the orifice centres, initiating 7 mm from the tank keel and 10 mm from the tank walls. The oscillatory kinematics were based on the guidelines published by Det Nørske Veritas (DNV) [2] and the Ship Structure Committee (SSC) [27] that consider the oscillatory response of cargo hold tanks undergoing different roll amplitudes, together with the resonant frequency, in relation to the tank properties utilised. The numerical analysis of the three tank models assumed 20%, 40%, and 60% fills within a maximum oscillatory displacement (θ_t) of 15° at frequencies of 0.5 Hz and 1.0 Hz.
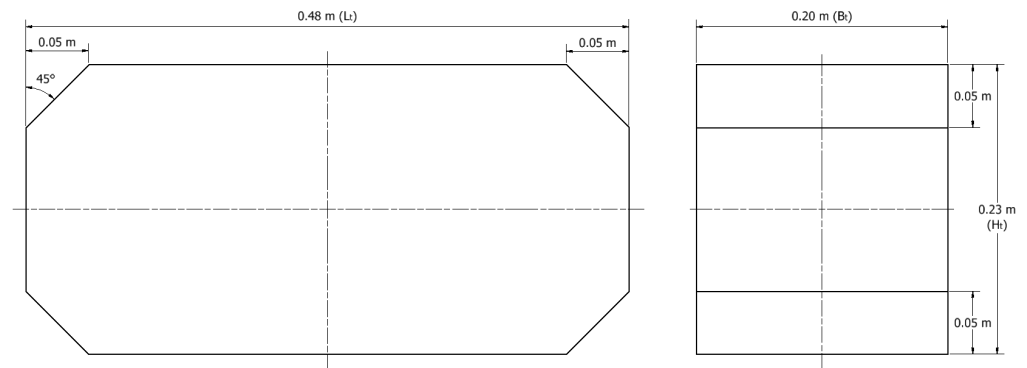

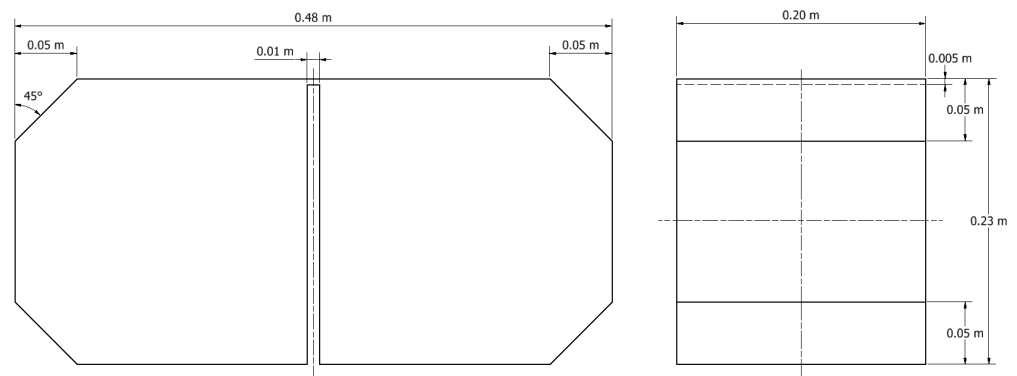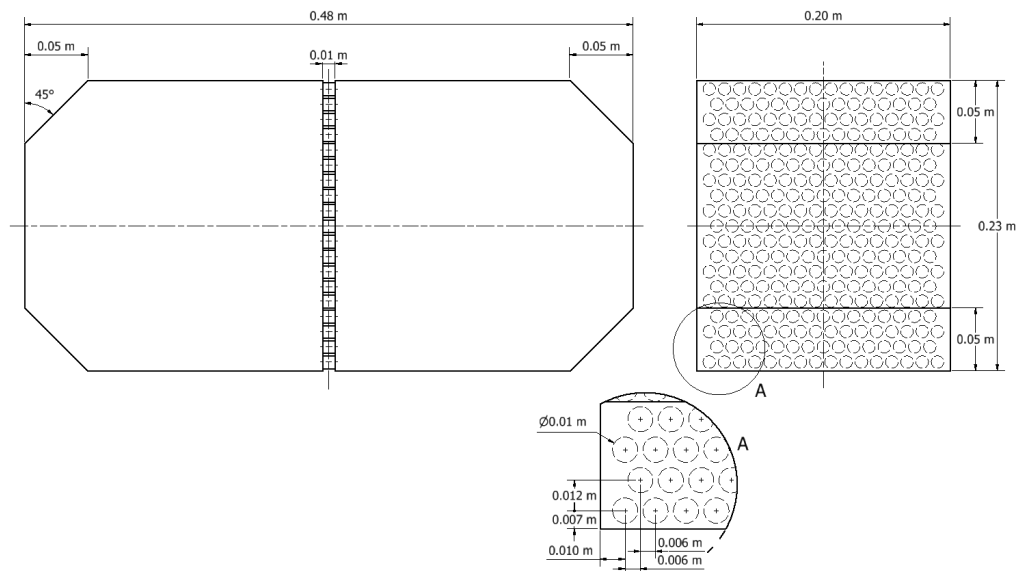**Figure 2.** First-angle projection of the open-bore tank geometrical model.

Figure 3. First-angle projection of the partitioned tank geometrical model.

Figure 4. First-angle projection of the perforated-partitioned tank geometrical model.

2.2. Computational Setup

The dam-break channel and sloshing-tank numerical models were solved utilising the VOF-CFD (volume-of-fluid computational fluid dynamics) methodology to track the multiphase free-surface. The commercial solver ANSYS-Fluent 19.2 was utilised in computing the continuity and Navier–Stokes equations. The Shear-Stress Transport (SST) k-ω Unsteady Reynolds-Averaged Navier–Stokes (URANS) turbulence model was implemented in mathematical closure to represent flow property fluctuation within the three-dimensional unsteady flow field.

The VOF scheme was utilised with explicit formulation volume fraction parameters, Sharp interface, and surface tension modelling. The non-iterative time-advancement (NITA) algorithm was utilised to diminish the total solution time [28]. The fractional step pressure-velocity coupling scheme was implemented with the Green-Gauss Node Based gradient, Pressure Staggering Option (PRESTO!) pressure, Second Order Upwind momentum, Geo-Reconstruct volume fraction, Second Order Upwind turbulent kinetic energy, and Second Order Upwind specific dissipation rate spatial discretisation schemes. The first order transient formulation scheme was utilised as the Explicit VOF model was implemented; second order models were hence inapplicable.

The full numerical domain of the dam-break wave represented the channel and reservoir. The no-slip wall condition was implemented upon the channel bed and rear plane. The pressure-outlet condition was allocated to the top and front planes. The symmetry condition was applied to the side planes. The domain was segregated into two cell-zones for distinct phase implementation, as illustrated in Figure 1. The tank domain surfaces were applied with the no-slip wall condition. Volumetric variations for phase implementation were induced within the solver by allocating distinct regions within the domain. Oscillatory kinetics were induced in the form of the simple pendulum equation of motion to numerically replicate a simple harmonic oscillator by means of a user-defined function (UDF) within a rotating-mesh model. A simulation was executed for 20 tank oscillation periods, where data acquisition was considered from the final 10 oscillations. The UDF is expressed in Appendix A. Furthermore, to establish sloshing impact zones, as defined in the ITTC sloshing guidelines [29], the tank geometric model surfaces were split to establish regions, illustrated in Figure 5 as highlighted surfaces, within which area-averaged static pressure data were acquired. The areas of the corner and middle surfaces were equivalent to 0.0066 m² and 0.0035 m², respectively.

A hexahedral mesh was imprinted upon the dam-break and sloshing-tank domains. To impose the hexahedral meshes, the dam-break and sloshing-tank domains were tactically segregated into cuboidal volumes within computer-aided design (CAD) software. A mesh independence procedure was carried out upon the dam-break validation model, described in Table 1, by considering the wave-tip displacement (x_s). The final domain mesh count was equivalent to 669,600 hexahedral volumetric cells. Subsequently, a mesh independence procedure was undertaken upon the open-bore tank, described in Table 2, acknowledging the maximum cycle-averaged torque (Q) induced at the highest degree of dynamics, 60% fill-level at 1 Hz. The final domain mesh count was equivalent to 1,008,640 hexahedral volumetric cells, resulting in an average cell volume of 0.1 cm³/cell; the final mesh is illustrated in Figure 5. The verified average cell volume was imposed on the supplementary tank domains. The meshes were imposed with a prism layer at no-slip surfaces with an appropriate cell height to achieve a y-plus (y^+) value of $30 \leqslant y^+ \leqslant 300$. The CFD computations were performed by running six Intel Core i7-7800X 3.50 GHz cores and 32 GB of RAM; a sloshing simulation was completed within an average of 55 wall-clock hours and 330 core-hours. Mesh independent parameters were established utilising ITTC recommended meshing procedures and guidelines [30]:

$$\varepsilon_{i_n} = S_{i_n} - S_{i_{n-1}} \tag{1}$$

$$R_i = \frac{\varepsilon_{i_n}}{\varepsilon_{i_{n-1}}} \tag{2}$$

where n is the mesh independence study iteration; R_i is the convergence ratio; ε_{i_n} is the difference between the considered variable (S_{i_n}); and r_i is the ratio between cell number iterations.

Table 1. Mesh independence analysis for the dam-break channel domain.

Cell Number	r_i	S_i	%$_{difference}$	ε_i	R_i
669,600	1.247	14.83	1.85	0.270	0.626
536,970	1.277	14.56	3.04	0.431	
420,500		14.13			

Table 2. Mesh independence analysis for the open-bore tank domain.

Cell Number	r_i	S_i	%$_{difference}$	ε_i	R_i
1,008,640	1.215	3.93	2.80	0.111	0.781
830,160	1.197	3.82	4.97	0.141	
693,530		3.63			
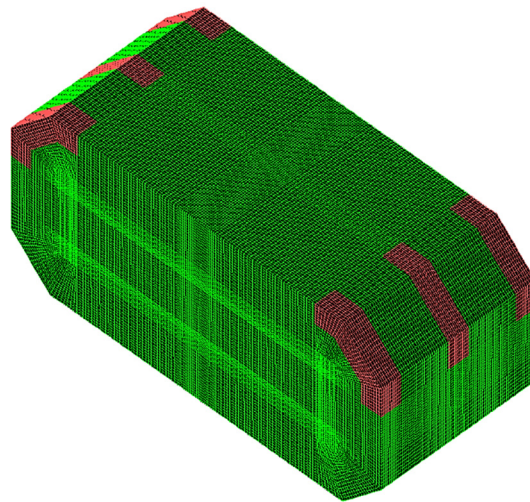
Figure 5. Meshed representation of the open-bore tank with highlighted surface zones for area-averaged static pressure data acquisition.

3. Numerical Model Characterisation

3.1. Physical Modelling

In establishing the validation model, the theoretical values for the dam-break wave-tip displacement and instantaneous free-surface wave profiles were acquired as derived by Chanson [26]. The frontal wave-tip displacement (x_s) was defined as:

$$x_s = H_r\left(\frac{3}{2}\frac{U_w}{\sqrt{gH_r}} - 1\right)\sqrt{\frac{g}{H_r}}t + \frac{32}{9}\left(\frac{2.5\text{ E-3}}{Re_{H_r}\frac{U_w}{\sqrt{gH_r}}}\right)^{-\frac{1}{4}}\left(\frac{U_w}{\sqrt{gH_r}}\right)^{-2}\left(1 - \frac{1}{2}\frac{U_w}{\sqrt{gH_r}}\right)^{\frac{9}{2}} \tag{3}$$

where H_r is the initial reservoir height; U_w is the wave-front celerity; g is the acceleration due to gravity; t is the elapsed time; $Re_{H_r} = \rho\sqrt{gH_r^3}/\mu$ is the dam-break Reynolds number; ρ is the fluid density; and μ is the fluid viscosity.

The free-surface wave profiles were defined as:

$$h_w = H_r, \ x \leq x_2 \tag{4a}$$

$$h_w = \frac{1}{9} H_r \left(2 - \frac{x}{t\sqrt{gH_r}} \right)^2, \ x_2 \leq x \leq x_1 \tag{4b}$$

$$h_w = \left(\frac{9}{32} H_r \left(\frac{2.5 \, \text{E-3}}{Re_{H_r} \frac{U_w}{\sqrt{gH_r}}} \right)^{\frac{1}{4}} \left(\frac{U_w}{\sqrt{gH_r}} \right)^2 \frac{x_s - x}{H_r} \right)^{\frac{4}{9}}, \ x_1 \leq x \leq x_s \tag{4c}$$

$$h_w = 0, \ x \geq x_s \tag{4d}$$

where h_w is the wave depth; x is the horizontal coordinate and x_1 and x_2 are characteristic locations.

In acknowledging standing wave sloshing motion within a rectangular cross-sectional tank, the resonance period (T_{res}) can be estimated as:

$$T_{res} = 2 \sqrt{\pi \frac{L_t}{g} \frac{1}{\tanh\left(\pi \frac{h}{L_t} \right)}} \tag{5}$$

where h is the tank-fill height.

Additionally, the sloshing torque coefficient (C_Q) was defined by the Ship Structure Committee [27] as:

$$C_Q = \frac{Q}{\rho g A_t L_t^2 \theta_t} \tag{6}$$

where Q is the torque generated by the fluid within the tank, and A_t is the frontal area of the tank. However, in variation of the oscillatory liquid-fill, the authors have derived the coefficient in relation to the static torque of a pendulum:

$$C_Q = \frac{Q}{\frac{I_t}{r} g \sin \theta_t} \tag{7}$$

where I_t is the liquid mass-moment of inertia and r is the displacement between the centre of rotation and liquid-mass centre of gravity; the two factors are variable with volume-fill.

Furthermore, the sloshing pressure coefficient (C_P) was defined by the Ship Structure Committee [27] as:

$$C_P = \frac{P}{\rho g L_t \theta_t} \tag{8}$$

where P is the static pressure generated by the fluid within the tank.

3.2. CFD Modelling

The conservation of mass and momentum were implemented within the CFD model in solving the flow domain:

$$\frac{\partial U_i}{\partial x_i} = 0 \tag{9}$$

$$\rho \frac{\partial U_i}{\partial t} + \rho U_j \frac{\partial U_i}{\partial x_j} = -\frac{\partial P_s}{\partial x_i} + \frac{\partial}{\partial x_j} \left(\mu \left(\frac{\partial U_i}{\partial x_j} + \frac{\partial U_i}{\partial x_j} \right) - \rho u_j' u_i' \right) \tag{10}$$

where U_i is the Reynolds-averaged velocity; x_i is the Cartesian coordinate; t is the elapsed time; P_s is the fluid static pressure; μ is the fluid dynamic viscosity; $-\rho u_j' u_i' = \rho \tau_{ij} = 2\mu_T S_{ij} - \frac{2}{3} \rho k \delta_{ij}$ is the Reynolds stress tensor and its assumption defined by the

Boussinesq eddy-viscosity approximation; μ_T is the eddy viscosity; S_{ij} is the mean strain-rate tensor; k is the turbulence kinetic energy; and δ_{ij} is the Kronecker delta. To close the momentum conservation equation, the SST k-ω turbulence model was implemented:

$$\rho \frac{\partial k}{\partial t} + \rho U_i \frac{\partial k}{\partial x_i} = \frac{\partial}{\partial x_j}\left[\Gamma_k \frac{\partial k}{\partial x_j}\right] + G_k - Y_k \tag{11}$$

$$\rho \frac{\partial \omega}{\partial t} + \rho U_i \frac{\partial \omega}{\partial x_i} = \frac{\partial}{\partial x_j}\left[\Gamma_\omega \frac{\partial \omega}{\partial x_j}\right] + G_\omega - Y_\omega \tag{12}$$

where ω is the specific dissipation rate; Γ_k and Γ_ω are the effective diffusivity of k and ω; G_k and G_ω are the generation of k and ω due to mean velocity gradients; and Y_k and Y_ω are the dissipation of k and ω due to turbulence [28].

4. Numerical Modelling Validation of a Turbulent Dam-Break Wave

In validating the multiphase VOF-CFD model, the numerical outcomes of a three-dimensional turbulent dam-break established the transient wave-tip displacement and free-surface wave profiles. The numerical outcomes were compared with the theoretical values estimated in Chanson [26]. The coefficient of determination (R^2) was determined.

The wave-tip displacement (x_s) numerical curve, illustrated in Figure 6, attained a coefficient of determination of 0.996 with the wave-tip displacement theoretical function (Equation (3)). Additionally, the free-surface numerical wave profiles (h_w) at 3, 6, 9, and 12 s plotted in Figure 7 attained R^2 values of 0.994, 0.995, 0.995, and 0.996, respectively, when compared with the theoretical free-surface wave profile function (Equation (4)). The implemented numerical schemes therefore attained very good comparison with the theoretical functions.
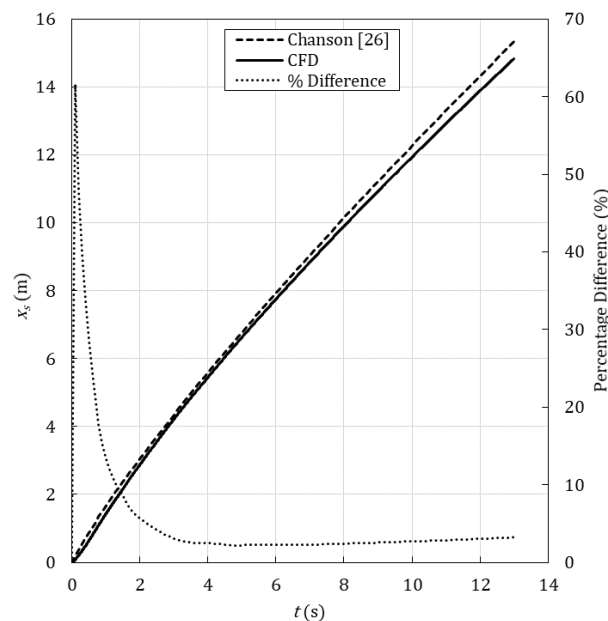
Figure 6. Dam-break wave-tip displacement (x_s) comparison between the CFD model and theoretical values derived by Chanson [26].

(a)

(b)

(c)

(d)
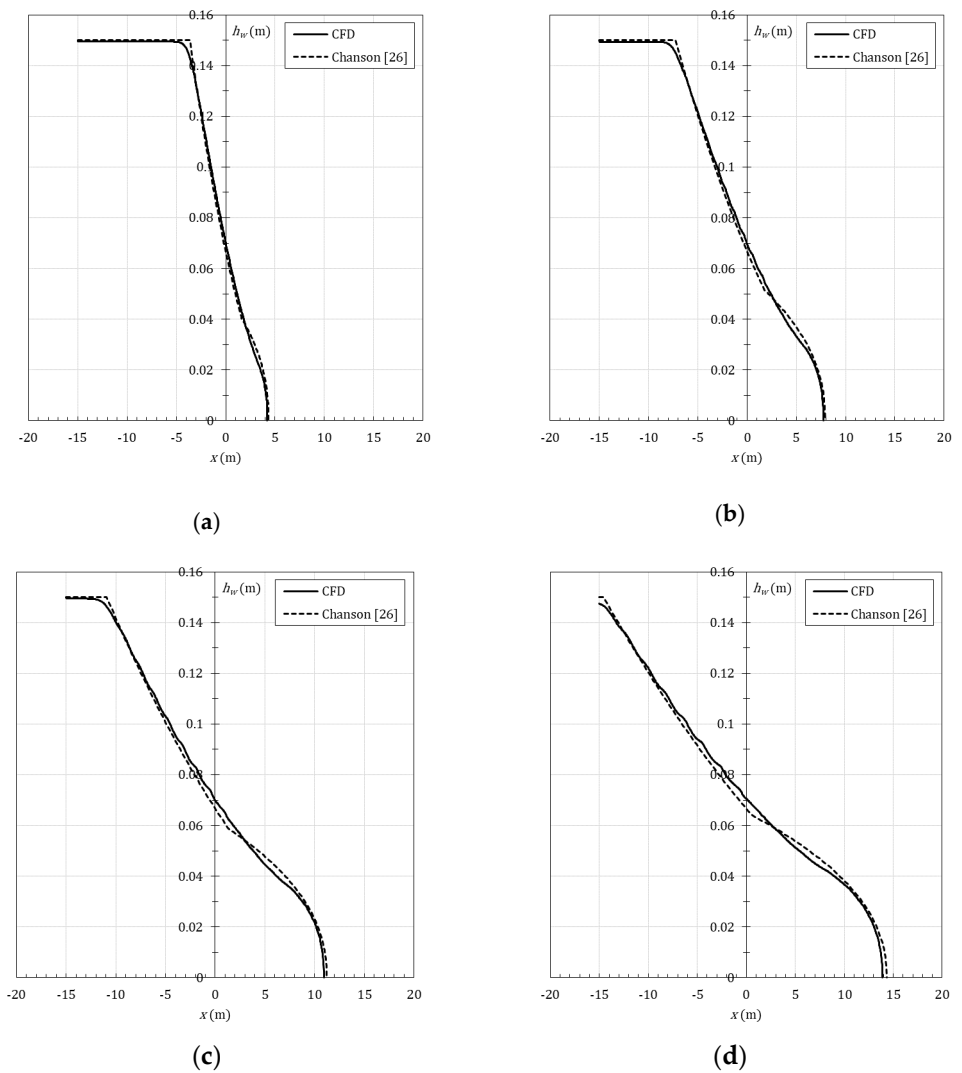
Figure 7. Dam-break free-surface wave profile (h_w) comparison between the CFD model and theoretical values derived by Chanson [26]. (**a**) $t = 3$ s. (**b**) $t = 6$ s. (**c**) $t = 9$ s. (**d**) $t = 12$ s.

5. Numerical Sloshing Performance of an Open-Bore, Partitioned, and Perforated-Partitioned Tank

To establish the performance of utilising an open-bore, a partitioned, and a perforated-partitioned tank, the period-averaged torque coefficient was analysed in relation to the tank angular displacement to determine acute variations in the data output, notably due to breaking-wave slamming impact. The period-averaging technique consisted of segregating the transient torque response by oscillation period, and averaging the period-synchronised response. Upon acknowledgement of slamming, the area-averaged static pressure at the critical tank locations proposed in Figure 3 was acquired to verify sloshing suppression performance.

5.1. 20% Fill

In analysing the resultant cycle-averaged torque at 20% fill, the response output, illustrated in Figure 8, exhibited a sigmoidal variation with angular displacement at both frequencies for all tank designs. At the fill-level, the sloshing dynamics within the partitioned and open-bore and perforated-partitioned tanks attained natural frequencies of 1.38 Hz and 0.711 Hz, respectively, utilising Equation (5). When oscillating at a frequency of 1 Hz, the open-bore response (Figure 8a) acquired a peak coefficient of ±0.90 at the

maximum angular displacement, with an increase to ±1.3 at a frequency of 0.5 Hz in approach towards the natural frequency. In comparison, the partitioned response (Figure 8b) attained relatively larger magnitudes of ±2.6 and ±1.8 at frequencies of 1 Hz and 0.5 Hz, respectively. The porous-partitioned response attained an intermediate coefficient of ±1.5 at both frequencies. The open-bore response was acknowledged to be lesser due to the momentum dissipation of the standing wave, generated per half-cycle of the oscillation, along the tank length. Due to the displacement suppression within the partitioned tank, the internal tank surface area at which a force may be produced increased, inducing a resultantly larger torque. The variation in torque coefficient at the oscillation dead-centre was established to be due to the minor shift in the liquid-body, accumulating towards the partition walls, producing larger forces. The porous-partitioned design similarly increased in surface area, but, due to the perforations, the liquid flowed through the partition, dissipating the dynamics, resulting in a wide-sigmoidal response (Figure 8c). Slamming due to breaking waves was not recognised.
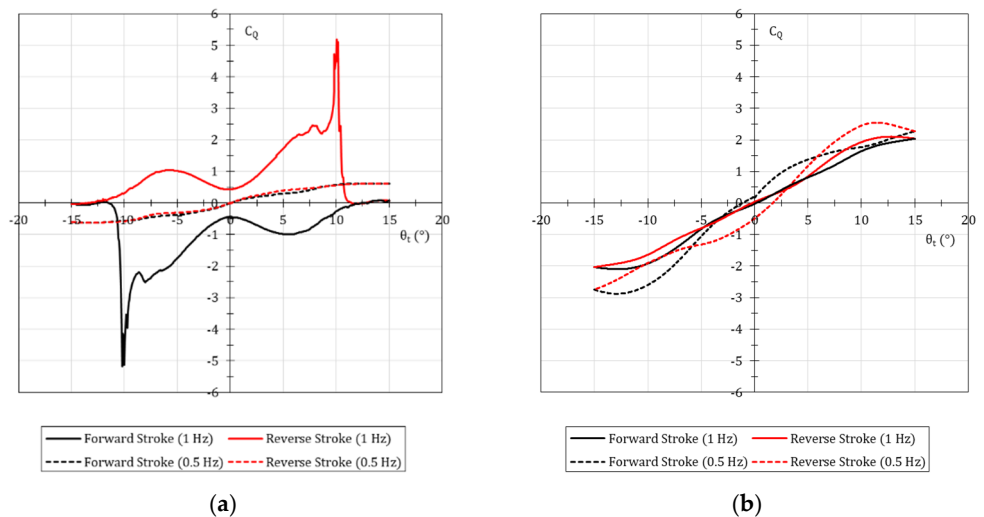

(a)

(b)

(c)
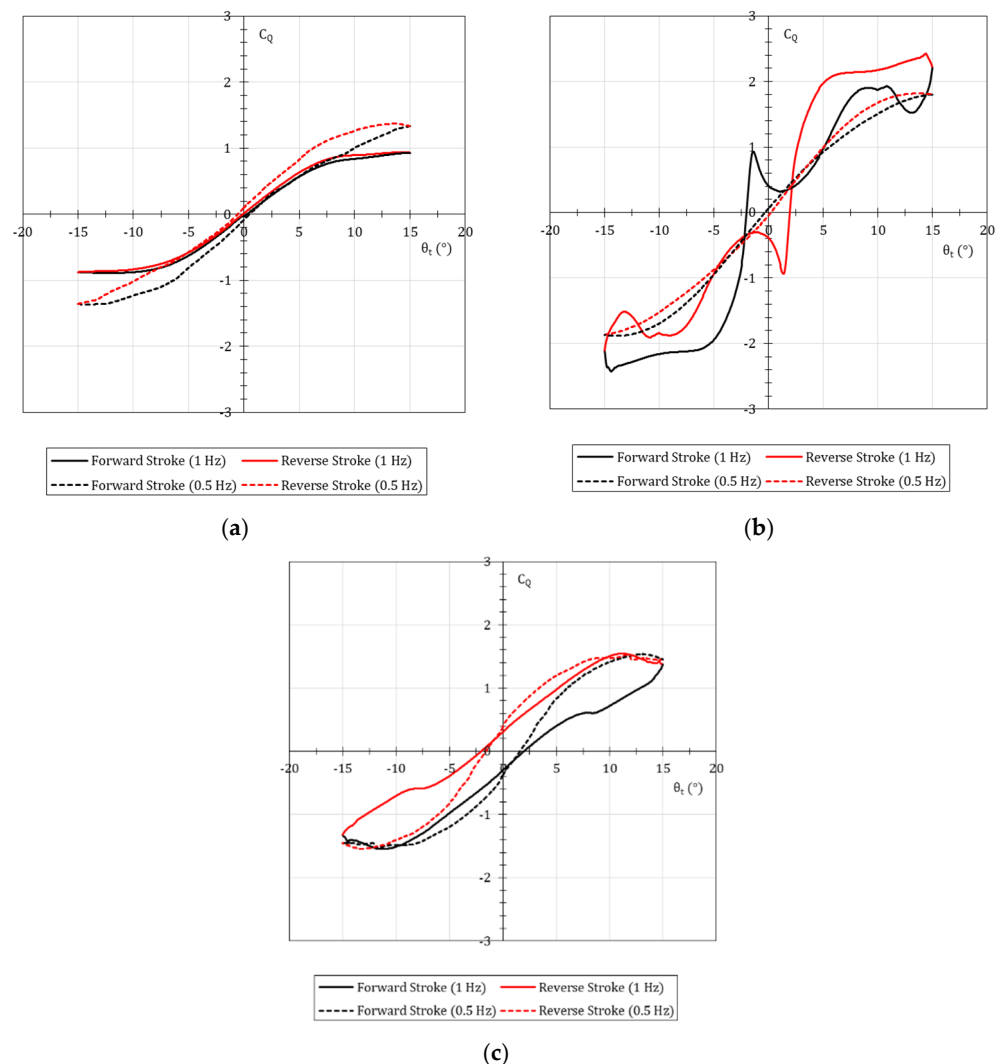
Figure 8. Cycle-averaged torque coefficient (C_Q) with angular displacement (θ_t) at 20% fill. (**a**) Open-bore. (**b**) Partitioned. (**c**) Perforated-partitioned.
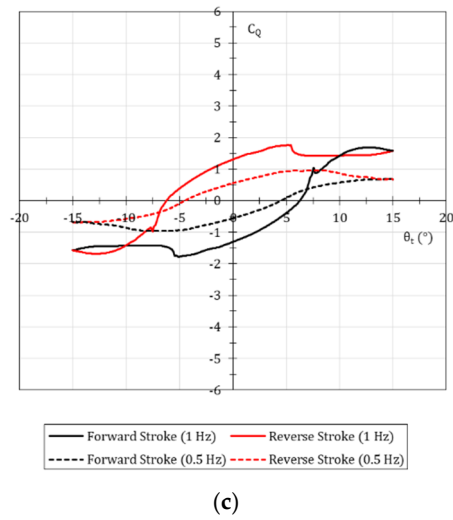
5.2. 40% Fill

In analysing the resultant cycle-averaged torque at 40% fill, the response output, illustrated in Figure 9, exhibited acute variations, suggesting breaking waves due to slosh-

ing. At the fill-level, the sloshing dynamics within the partitioned and open-bore and per-forated-partitioned tanks attained natural frequencies of 0.94 Hz and 1.67 Hz, respectively. When oscillating at a frequency of 1 Hz, the open-bore response (Figure 9a) acquired a peak coefficient of ±5.25 at an angular displacement of ±10°. The acute rise in the torque response indicated the presence of liquid slamming within the tank as the induced oscillation frequency was equivalent to the theoretical natural frequency. The slamming effect was recognised to occur at the initial stage of an oscillation stroke. Therefore, upon oscillating towards the maximum angular displacement, the liquid-shift impact occurred subsequent to the tank kinematic change in direction, and was hence asynchronous to the tank kinetics by 5°. The response decreased to ±0.6 at a frequency of 0.5 Hz. In comparison, the partitioned response (Figure 9b) attained consistent magnitudes of ±2.1 and ±2.5 at frequencies of 1 Hz and 0.5 Hz, respectively. The porous-partitioned response (Figure 9c) attained coefficients of ±1.75 and ±0.8 at 1 Hz and 0.5 Hz, respectively, within a wide sigmoidal response. The unique response at 40% fill-volume presented an advantage of utilising perforated-partitions in diminishing sloshing dynamics. The presence of the barrier suppressed momentum production of the wave throughout the liquid-shift. However, due to the perforations, the wave dynamics were diffused and dissipated through the multiple orifices, thereby attaining a lesser torque response in comparison to the open-bore and partitioned tank designs.

As slamming due to breaking waves was recognised, the cycle-averaged, area-averaged static pressure at the chamfered junction of the tank keel and tank port and starboard walls was analysed (Figure 10). The pressure at each chamfered segment was established to peak twice per cycle, attaining a primary peak coefficient of 0.13 at an angular displacement of ±7° and a secondary peak coefficient of 0.055 at an angular displacement of ±6°. As a result, as the tank finalised the reverse stroke and initiated the forward stroke, the liquid slosh therefore impacted the tank wall whilst the tank motion was the opposite to that of the wave, at an angular displacement of −10°, which proceeded to impact the locations of interest at a displacement of −7° and 6° within the same stroke.

(a)   (b)

(**c**)

Figure 9. Cycle-averaged torque coefficient (C_Q) with angular displacement (θ_t) at 40% fill. (**a**) Open-bore. (**b**) Partitioned. (**c**) Perforated-partitioned.
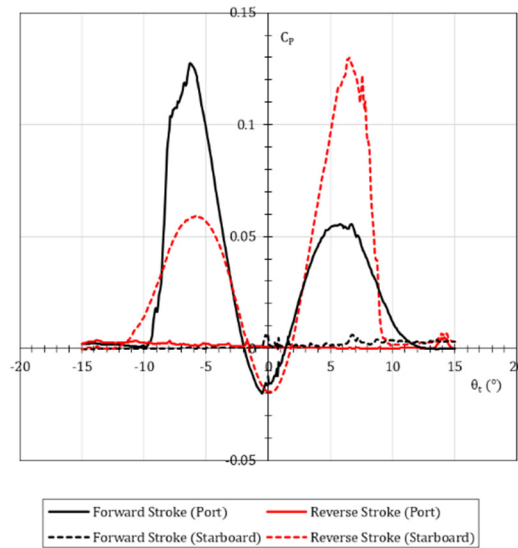

Figure 10. Cycle-averaged pressure coefficient (C_P) with angular displacement (θ_t) of the open-bore tank at 40% fill.

In establishing the variation in the sloshing wave movements within the open-bore, partitioned, and perforated-partitioned tanks at 40% fill, contours of volume phase at quarter cycles within one oscillation was recognised, as illustrated in Figures 11–13. The transient effect of the slosh dynamics upon impact was distinctively variant between the three tank designs.
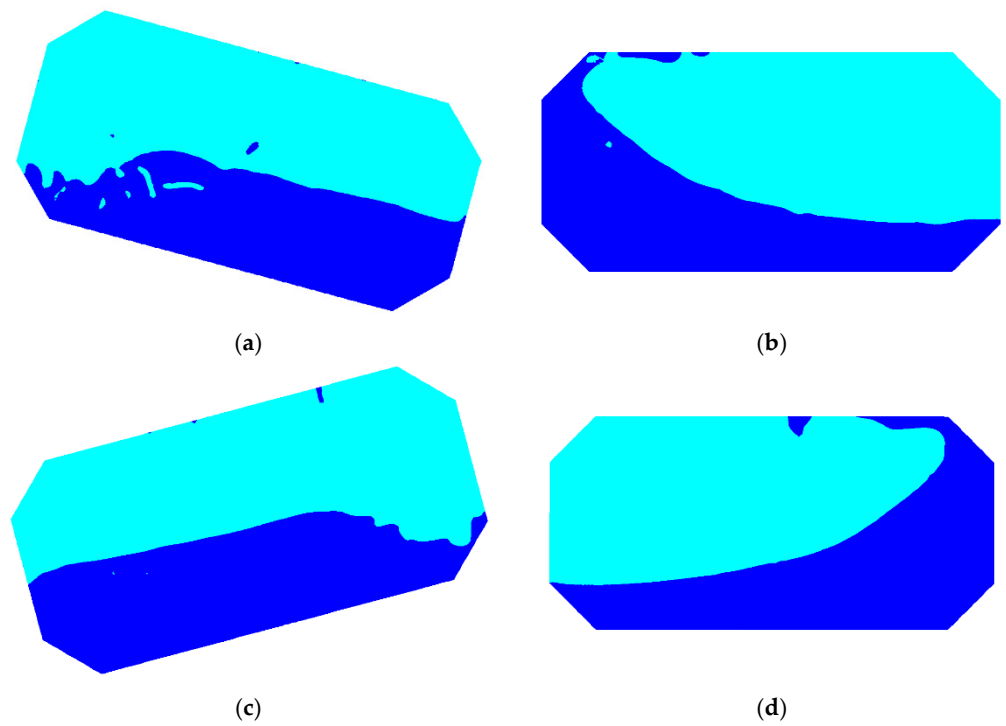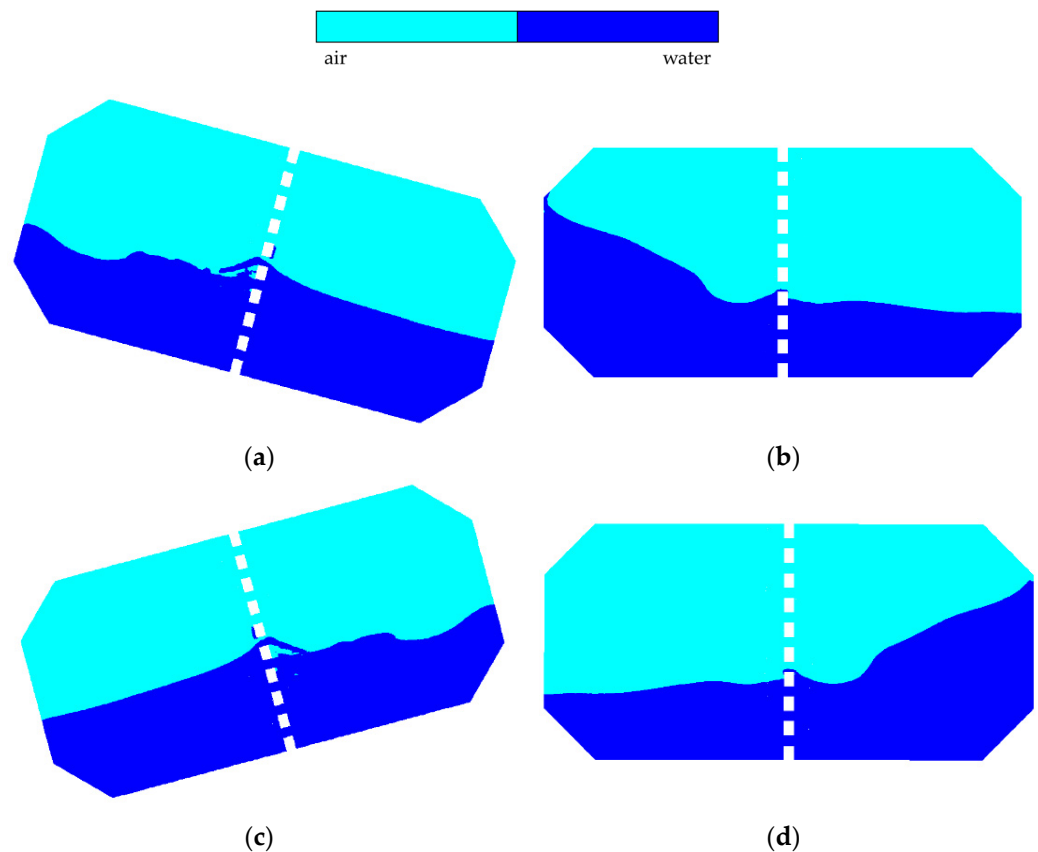
Figure 11. Cross-sectional contoured illustrations of the sloshing dynamics within the open-bore tank at 40% fill. (**a**) $\theta_t = -15°$ (initial position). (**b**) $\theta_t = 0°$ (quarter-stroke). (**c**) $\theta_t = 15°$ (mid-stroke). (**d**) $\theta_t = 0°$ (three-quarter-stroke).
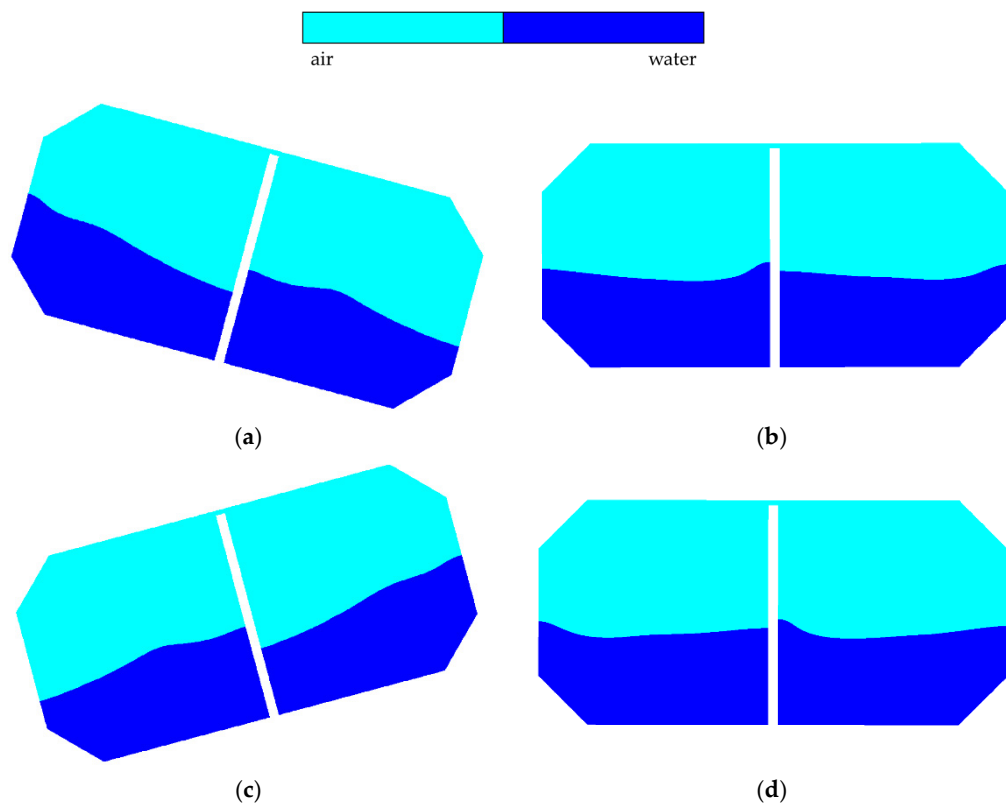
Figure 12. Cross-sectional contoured illustrations of the sloshing dynamics within the partitioned tank at 40% fill. (**a**) $\theta_t = -15°$ (initial position). (**b**) $\theta_t = 0°$ (quarter-stroke). (**c**) $\theta_t = 15°$ (mid-stroke). (**d**) $\theta_t = 0°$ (three-quarter-stroke).

Figure 13. Cross-sectional contoured illustrations of the sloshing dynamics within the perforated-partitioned tank at 40% fill. (**a**) $\theta_t = -15°$ (initial position). (**b**) $\theta_t = 0°$ (quarter-stroke). (**c**) $\theta_t = 15°$ (mid-stroke). (**d**) $\theta_t = 0°$ (three-quarter-stroke).
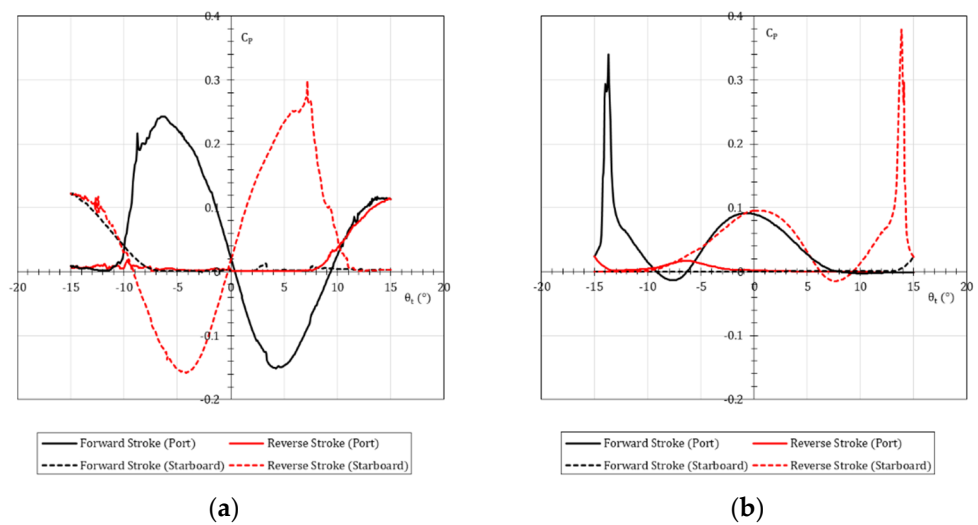
5.3. 60% Fill

In analysing the resultant cycle-averaged torque at 60% fill, the response output, illustrated in Figure 14, exhibited acute variations, suggesting breaking waves due to sloshing. At the fill-level, the sloshing dynamics within the partitioned and open-bore and perforated-partitioned tanks attained natural frequencies of 1.08 Hz and 1.78 Hz, respectively. When oscillating at a frequency of 1 Hz, the open-bore response (Figure 14a) acquired a peak coefficient of ±1.6 at an angular displacement of ±6°. Subsequently, within one-third of a cycle, the torque coefficient varied to ±1.3, establishing a torque coefficient discrepancy of 2.9. The substantial variation in magnitude and orientation of torque was manifested as a result of high-energy wave slamming at the tank walls and tank keel, at which the slosh wave ricocheted towards the opposite tank side, imposing an opposing torque. The elaboration was seconded in Figure 15a, illustrating the static pressure coefficient at the chamfered locations. As the tank oscillated from dead-centre (0°) to maximum negative angular displacement (−15°) along the forward stroke, the slosh wave impacted port-side whilst the tank was at a displacement of −5°. Subsequently, as the tank approached a displacement of −15°, the static pressure at the starboard-side increased. The wave therefore underwent slamming at one side of the tank, and ricocheted towards the opposite tank side within a tank angular discrepancy of 10°. The pressure at each chamfered segment was established to peak twice per cycle. A peak torque coefficient of 1.2 was attained at an oscillatory frequency of 0.5 Hz.

In comparison, the partitioned response (Figure 14b) attained magnitudes of ±1.3 and ±2.1, in a sigmoidal variation, at frequencies of 1 Hz and 0.5 Hz, respectively. The perforated-partition response (Figure 14c) established acute variations in torque at an angular displacement of ±14° to a coefficient value of ±2.9. In contrast to the response at 40% fill, the perforated-partition did not introduce sufficient dissipation of the wave momentum

to abolish the occurrence of slamming due to breaking waves, but prevented the sloshing ricochet dynamics acknowledged within an open-bore tank at 60% fill from occurring. As slamming due to breaking waves was detected, the cycle-averaged, area-averaged static pressure at the chamfered junction of the tank keel and tank port and starboard walls was analysed (Figure 15). The pressure at each chamfered segment was established to peak twice per cycle, attaining a primary peak coefficient of 0.36 at an angular displacement of ±14° and a secondary peak coefficient of 0.9 at tank dead-centre.

(**a**)

(**b**)

(**c**)
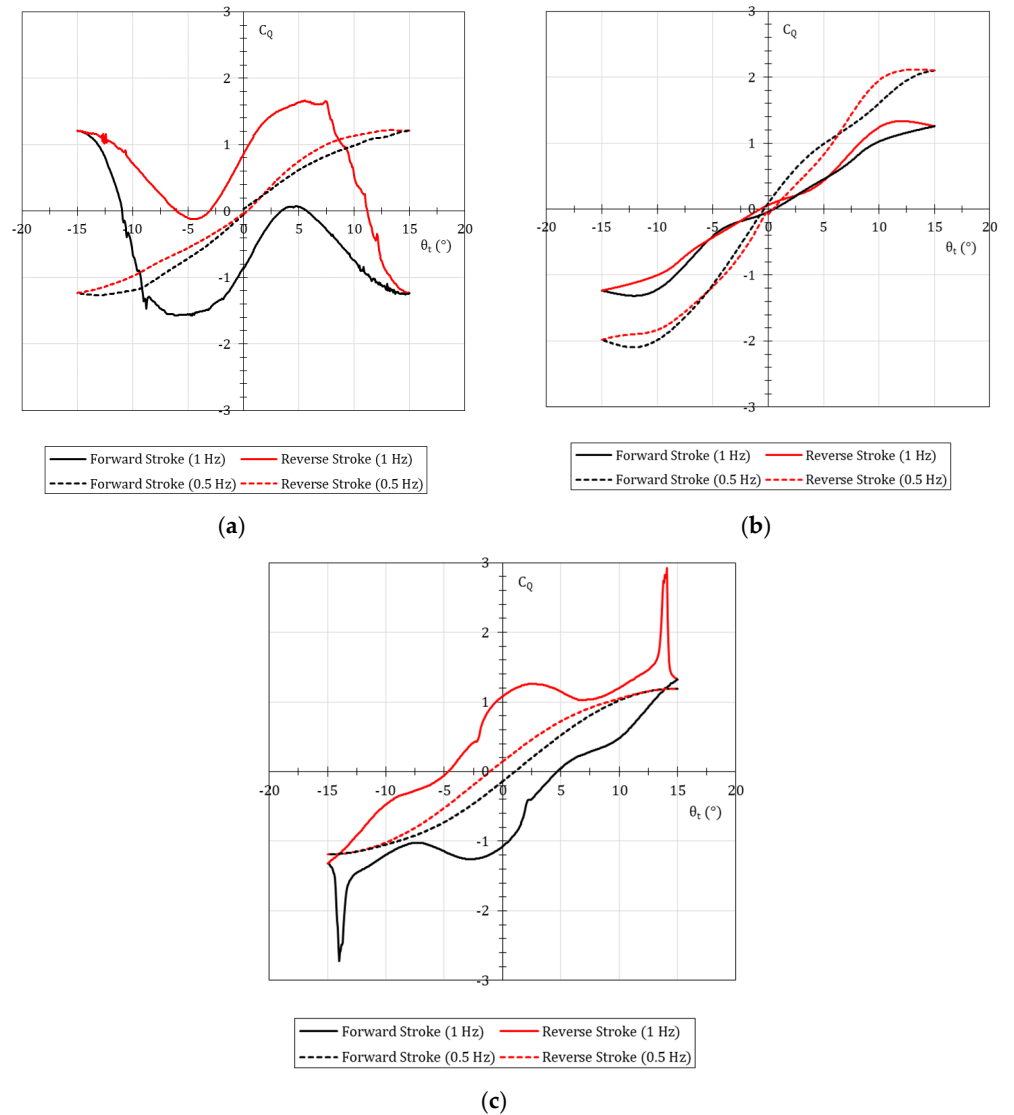
Figure 14. Cycle-averaged torque coefficient (C_Q) with angular displacement (θ_t) at 60% fill. (**a**) Open-bore. (**b**) Partitioned. (**c**) Perforated-partitioned.

Figure 15. Cycle-averaged pressure coefficient (C_P) with angular displacement (θ_t) at 60% fill. (**a**) Open-bore. (**b**) Perforated-partitioned.

6. Discussion

Throughout transportation of the liquid cargo within partially-filled tanks, violent ship motions due to adverse weather conditions along shipping routes may induce substantial dynamic variation upon the contained cargo, detrimentally affecting vessel seakeeping and manoeuvrability. Significant sloshing dynamics within liquefied natural gas cargo tanks materialise as breaking waves, potentially bringing about containment structural damage and stability loss due to high-impact slamming. Thus, tank-fill limitations have been acknowledged as precautions to prevent engineering repercussions due to sloshing, imposing cargo volume-fill limitations to be either lower than 10% or higher than 70% of the tank height. In recognition of the restrictions, three distinct tank designs with partitions of different porosities were put forward to investigate the sloshing-suppression performance of an open-bore (100% porosity), partitioned (0% porosity), and a perforated-partitioned (50% porosity) tank at 20%, 40%, and 60% volume-fills within a pendulum-oscillatory setup.

Investigating acute discrepancies in torque output to determine wave slamming at the tank keel, the period-averaged torque coefficient induced was established to vary in a sigmoidal manner with oscillatory angular displacement. At 20% fill, the operating frequency acted distant from the natural frequency where sloshing wave slamming was not present due to wave dissipation within the open-bore and perforated-partitioned tank, together with wave suppression within the partitioned tank. At 40% fill, slamming at the tank keel occurred within the open-bore setup as the operating frequency was equivalent to the natural frequency. Given the frequency equivalence, the perforated-partition succeeded in dissipating the sloshing wave, dampening the fluid dynamics. At 60% fill, slamming occurred within both the open-bore and perforated-partition tank, but the sloshing dynamics varied significantly. The damping factor induced by the perforation installation therefore altered, but insufficiently hindered, the sloshing conditions. The analyses, however, put forward the efficacy of tank perforated-partitions upon dynamic sloshing reduction as an internal design feature for liquid-cargo containment units.

7. Conclusion

The study put forward a computational fluid dynamic sloshing analysis of partially-filled chamfered rectangular tanks undergoing sinusoidal oscillatory kinetics with the use of the explicit volume-of-fluid and non-iterative time-advancement schemes utilising the commercial solver ANSYS-Fluent. Within a 20% to 60% fill-range, the sloshing dynamics were acknowledged within an open-bore, partitioned, and perforated-partitioned tank

when oscillating at frequencies of 0.5 Hz and 1 Hz. The overall torque and static pressure induced on the tank walls were investigated. High-impact slamming at the tank roof occurred at 40% and 60% fills, but the implementation of the partition and perforated-partition barriers successfully reduced the impact due to suppression and dissipation of the wave dynamics.

Institutional Review Board Statement: Not applicable.

Informed Consent Statement: Not applicable.

Data Availability Statement: Not applicable.

Conflicts of Interest: The authors declare no conflicts of interest.

Appendix A

The ANSYS-Fluent user-defined function (UDF) macro utilised to implement oscillatory kinematics when coupled with the moving-mesh model is defined as:

```
#include "udf.h"

DEFINE_ZONE_MOTION(fmotion,omega,axis,origin,velocity,time,dtime)
{
  double A_r;
  double freq_n;
  double pi;

  pi = 3.14159265359;

  A_r = 0.2618;            /* maximum angular tank displacement (in radians) */
  freq_n = 1.00;           /* oscillatory frequency (in Hz)*/

  *omega = A_r · (2 · pi · freq_n) · cos(2 · pi · freq_n · time); /* oscillatory formula */

  N3V_D(velocity, =, 0.0, 0.0, 0.0);         /* linear velocity */
  N3V_D(origin, =, 0.0, 0.22, 0.0);          /* pivot origin */
  N3V_D(axis, =, 0.0, 0.0, 1.0);             /* rotational axis */

  return;
}
```

In elaboration of the UDF, the DEFINE macro was coupled to the domain cell zone to induce a zone motion. Upon definition of the variables/constants required, the oscillatory formula expressing the rotational velocity of a pendulum was imposed. Three vectors defining the linear velocity, pivot origin, and rotational axis were then put forward.

References

1.   Olsen, H. What is Sloshing? In *Seminar on Liquid Sloshing*; Den Nørske Veritas (DNV): Hovik, Norway, 1976.

2. Det Nørske Veritas (DNV). *DNVGL-CG-0158 Sloshing Analysis of LNG Membrane Tanks*; Technical report; Den Nørske Veritas (DNV): Hovik, Norway, 2016.

3. Türk Loydu. *S.P 01/20 Guidelines for the Assessment of Sloshing Impact Loads*; Technical report; 2020. https://turkloydu.org/pdf-files/teknik-sirkulerler/tekne/S-P-01-20.pdf (accessed on 18 January 2022)

4. Budiansky, B. Sloshing of Liquids in Circular Canals and Spherical Tanks. *J. Aero/Space Sci.* **1960**, *27*, 161–173.

5. Abramson, H. *The Dynamic Behavior of Liquids in Moving Containers, with Applications to Space Vehicle Technology*; Technical Report; National Aeronautics and Space Administration (NASA): Washington, DC, USA, 1966.

6. Slibar, A.; Troger, H. The Steady State Behaviour of Tank Trailer System carrying Rigid or Liquid Cargo. *Veh. Syst. Dyn.* **1977**, *6*, 167–169.

7. Ranganathan, R. Rollover Threshold of Partially Filled Tank Vehicles with Arbitrary Tank Geometry. *J. Automot. Eng.* **1993**, *207*, 241–244.

8. Salem, M.I.; Mucino, V.H.; Saunders, E.; Gautam, M.; Lozano-Guzman, A. Lateral sloshing in partially filled elliptical tanker trucks using a trammel pendulum. *Int. J. Heavy Veh. Syst.* **2009**, *16*, 207–224.

9. Gabl, R.; Davey, T.; Ingram, D.M. Roll Motion of a Water Filled Floating Cylinder—Additional Experimental Verification. *Water* **2020**, *12*, 2219.

10. Celebi, M.S.; Akyildiz, H. Nonlinear modeling of liquid sloshing in a moving rectangular tank. *Ocean Eng.* **2002**, *29*, 1527–1553.

11. Akyildiz, H. A numerical study of the effects of the vertical baffle on liquid sloshing in two-dimensional rectangular tank. *J. Sound Vib.* **2012**, *331*, 41–52.

12. He, T.; Feng, D.; Liu, L.; Wang, X.; Jiang, H. CFD Simulation and Experimental Study on Coupled Motion Response of Ship with Tank in Beam Waves. *J. Mar. Sci. Eng.* **2022**, *10*, 113.

13. Bulian, G.; Botia-Vera, E.; Mas-Soler, J.; Souto-Iglesias, A.; Castellana, F.; Repeatability and Practical Ergodicity of 2D Sloshing Experiments. Proceedings of the Twenty-second International Offshore and Polar Engineering Conference, Rhodes, Greece, June 2012.

14. Thiagarajan, K.P.; Rakshit, D.; Repalle, N. The air–water sloshing problem: Fundamental analysis and parametric studies on excitation and fill levels. *Ocean Eng.* **2011**, *38*, 498–508.

15. Tao, K.; Zhou, X.; Ren, H. A Novel Improved Coupled Dynamic Solid Boundary Treatment for 2D Fluid Sloshing Simulation. *J. Mar. Sci. Eng.* **2021**, *9*, 1395.

16. Jiang, H.; You, Y.; Hu, Z.; Zheng, X.; Ma, Q. Comparative Study on Violent Sloshing with Water Jet Flows by Using the ISPH Method. *Water* **2019**, *11*, 2590.

17. Trimulyono, A.; Hashimoto, H.; Matsuda, A. Experimental Validation of Single- and Two-Phase Smoothed Particle Hydrodynamics on Sloshing in a Prismatic Tank. *J. Mar. Sci. Eng.* **2019**, *7*, 247.

18. Liu, D.; Lin, P. Three-dimensional liquid sloshing in a tank with baffles. *Ocean Eng.* **2009**, *36*, 202–212.

19. Jung, J.H.; Yoon, H.S.; Lee, C.Y.; Shin, S.C. Effect of the vertical baffle height on the liquid sloshing in a three-dimensional rectangular tank. *Ocean Eng.* **2009**, *44*, 79–89.

20. Yu, Y.-M.; Ma, N.; Fan, S.-M.; Gu, X.-C. Experimental and numerical studies on sloshing in a membrane-type LNG tank with two floating plates. *Ocean Eng.* **2017**, *129*, 217–227.

21. Lin, L.; Jiang, S.; Zhao, M.; Tang, G. Two-dimensional viscous numerical simulation of liquid sloshing in rectangular tank with/without baffles and comparison with potential flow solutions. *Ocean Eng.* **2015**, *108*, 662–677.

22. Molin, B. Hydrodynamics Modeling of Perforated Structures. *Appl. Ocean Res.* **2011**, *33*, 1–11.

23. Faltisen, O. M.; Firoozkoohi, R.; Timokha, A. N. Steady-State Liquid Sloshing in a Rectangular Tank with a Slat-Type Screen in the Middle: Quasilinear Modal Analysis and Experiments. *Phys. Fluids* **2011**, *23*, 042101.

24. Molin, B.; Remy, F. Experimental and Numerical Study of the Sloshing Motion in a Rectangular Tank with a Perforated Screen. *J. Fluids Struct.* **2013**, *43*, 463–480.

25. Jin, H.; Liu, Y.; Li, H.-J. Experimental Study on Sloshing in a Tank with an Inner Horizontal Perforated Plate. *Ocean Eng.* **2014**, *82*, 75–84.

26. Chanson, H. Application of the method of characteristics to the dam break wave problem. *J. Hydraul. Res.* **2009**, *47*, 41–49.

27. Ship Structure Committee (SSC). *SSC-336 Liquid Sloshing in Cargo Tanks*; Technical report; Ship Structure Committee: Washington, DC, USA, 1990.

28. ANSYS Inc. *FLUENT User's Guide*, 5th ed.; ANSYS Inc.: Lebanon, NH, USA, 1998.

29. Seakeeping Committee of the 28th ITTC. Recommended Procedures and Guidelines: Sloshing Model Tests. Technical Report. 2017. https://www.ittc.info/media/8111/75-02-07-027.pdf (accessed on 18 January 2022)

30. Resistance Committee of the 28th ITTC. Recommended Procedures and Guidelines: Uncertainty Analysis in CFD Verification and Validation Methodology and Procedures. Technical Report. 2017. https://www.ittc.info/media/8153/75-03-01-01.pdf (accessed on 18 January 2022)